Effect of Hydrogen Bonding on Characterization of Polyamide 612 and Ethylene Vinyl Alcohol Copolymer Blends

Li Cui,[1] Zhi-Chao Wang,[2] Ping Zhu,[1] Jen-Taut Yeh[1]

[1]*Key Laboratory of Green Processing and Functional Textiles of New Textile Materials, Wuhan Textile University, Ministry of Education, Wuhan, China*
[2]*Department of Computer Software, College of Information Engineering, Wuhan University of Science and Technology Zhongnan Branch, Wuhan, China*

Received 2 July 2010; accepted 11 October 2010
DOI 10.1002/app.33593
Published online 14 February 2011 in Wiley Online Library (wileyonlinelibrary.com).

ABSTRACT: Hydrogen bonding interaction in the blends of polyamide 612 (PA^{612})/ethylene vinyl alcohol copolymer (EVOH) and the effect of the hydrogen bonds on the characterization of PA^{612}/EVOH were investigated. Fourier transform infrared spectra (FTIR) analysis indicated that the interactions between the carbonyl groups of PA^{612} and hydroxyl groups of EVOH increase as the content of EVOH in PA^{612}/EVOH specimens increase. This interaction between PA^{612} and EVOH leads to their miscibility to some extent in the amorphous region and even some effects on their crystal phase, respectively. Further isothermal crystallization behavior of PA^{612}/EVOH indicates that the hydrogen bonding between PA^{612} and EVOH leading difficulty in crystallization of PA^{612}. Several kinetics equations are employed to describe the effects of EVOH on the crystallization properties of PA^{612} in PA^{612}/EVOH blends in detail. © 2011 Wiley Periodicals, Inc. J Appl Polym Sci 120: 3724–3732, 2011

Key words: polyamide 612; ethylene vinyl alcohol copolymer; crystallization; hydrogen bond

INTRODUCTION

There has been considerable interest in polymer blends in recent decades, owing to their better combination of physical properties and potential applications than those of the homo-polymers.[1–3] It is generally recognized that the properties of polymer blends are greatly dependent on their miscibility and phase behavior. Therefore, the phase behavior of polymer blends has been the subject of numerous studies.[4–8]

Several studies[5–9] have appeared in the literature concerning the compatibility of polyamides with polymers containing vinyl alcohol monomer units, which are capable of hydrogen-bond interactions. It is well-known that most polymer blends are miscible due to the hydrogen bonding interaction. This type of interaction has been widely described in terms of association model by Coleman et al.[10,11] This model is modified by the Flory-Huggins theory to include a free energy change associated with hydrogen bonding that has both entropic and enthalpic contribution.[10–14] Many researchers, such as Kwei,[15,16] Chang,[17–19] and Habi,[20,21] carried out the effect of hydrogen bonding on the miscibility of polymer, and found that the properties of polymer blends are greatly dependent on their miscibility. Coleman and Painter[22] suggest that hydrogen bonding, which is very complicated in ethylene-vinyl alcohol copolymer (EVOH) and involves an extraordinary variety of inter and intramolecular species, plays an important role in the phase behavior of EVOH/polyamide 6 (PA6) blends. Ha and Ko[23] explained that EVOH/nylon 46 blends are miscible at concentrations below 35 wt % of nylon 46, and the blends have strong intermolecular interaction between the C—O group of EVOH and the *N*-H group in nylon 46 as the nylon 46 contents are less than 35 wt %. In our recent investigation,[24] it was found that the hydrogen bonding interaction between PA6 and Poly(vinyl alcohol) leads to their miscibility in the amorphous state and even some extent effects on their crystal phase. In some blends, the hydrogen bonds are so strong that the crystallization of the crystalline component is totally prohibited when its content is low. For example, poly(hydroxy valerate) (PHV) was completely prevented from crystallization in its blends with poly(*p*-vinylphenol) (PVPh) for PHV content lower than 50wt%.[25] In poly(Hydroxy Butyrate) (PHB)/PVPh blends, PHB loses its crystallizability in the presence of 40 wt % PVPh.[26] Also, polycaprolactone (PCL), a semicrystalline polymer in the pure state,

Correspondence to: L. Cui (cuili027@foxmail.com).

exists as a fully amorphous elastomer in PCL/dihydric phenol blends with dihydric phenol content higher than 40 wt %.[27,28] Hydrogen bonds can also affect the crystalline polymorphic form of crystalline components. For example, in the poly(vinylidene fluoride) (PVDF)/ polyvinyl pyrrolidone (PVP) blend with low PVP content, the specific interaction between segmental PVDF and PVP transforms the crystalline state of PVDF from α to γ phase.[29]

EVOH is always recognized as an oxygen-barrier material in food and other packaging applications that require protection from oxygen for its superior gas barrier property and high oil resistance.[30] However, the blends of EVOH with mass kinds of polyamides are easy to absorb moisture and so reduce its merit. On the other hand, although polyamide 612 (PA^{612}) exhibits some general property as polyamide, PA^{612} typically absorbs much less moisture than PA6 or PA66 and therefore has better dimensional stability and electric capability than polyamide 6 (PA6) or polyamide 66 (PA66).[31] However, the barrier property of PA^{612} is worse than PA6 resin. To investigate a novel material with lower moisture absorption and higher gas and oil resistance, EVOH resin whose barrier property is even better than PA6 was added in PA^{612} resin. This novel material is expected to be used as packaging, tank, and battery box, etc. As far as we know, the hydrogen bonding interaction and moisture absorption properties of blends of PA^{612} and EVOH have never been reported.

It is well understood that the physical, chemical, and mechanical properties of crystalline polymers depend on morphology, crystalline structure, and crystallinity. To control the rate of the crystallization and the degree of crystallinity and to obtain the desired morphology and properties, a great deal of effort has been devoted into studying the crystallization kinetics and determining the change in material properties. In this study, molecular interaction between PA^{612} and EVOH in PA^{612}/EVOH blends is investigated by Fourier transform infrared spectroscopy (FTIR). The effects of hydrogen bonding in PA^{612}/EVOH blends on the miscibility in the amorphous region and crystal properties of PA^{612}/EVOH blends are studied in detail by wide angle X-ray diffraction, dynamic mechanical, and isothermal crystallization analysis of PA^{612}/EVOH specimens.

EXPERIMENTAL

Materials and sample preparation

EVOH with 32 mol percentage ethylene content and PA612 (PA^{612}) with the trade name of 151LNC-10 resins used in this study were obtained from Kuraray Corp. (Osaka, Japan) and Du Pont (Wilmington, USA) corps, respectively.

TABLE I
Compositions of PA^{612}/EVOH Specimens Prepared in This Study

Sample	PA^{612} (wt%)	EVOH (wt %)
PA^{612}	100	0
$PA^{612}{}_7EVOH_1$	87.5	12.5
$PA^{612}{}_5EVOH_1$	83.3	16.7
$PA^{612}{}_3EVOH_1$	75.0	25.0
$PA^{612}{}_1EVOH_1$	50.0	50.0

The PA^{612}/EVOH specimens were prepared by melt blending the PA^{612} and EVOH resins using a SU-70 Plasti-Corder Mixer (Suyuan Science and Technology Co., Changzhou, China). Before melt-blending, the PA^{612} and EVOH resins were dried in a vacuum oven at 80°C for 16 and 12 h, respectively. The dried components of PA^{612}/EVOH at varying weight ratios were then melt-blended in the Plasti-Corder Mixer. During each melt-blending process, the Plasti-Corder Mixer instrument was operated at 230°C and a screw speed of 250 rpm for 4 min. The compositions of the PA^{612}/EVOH specimens prepared in this study are summarized in Table I. The prepared PA^{612}/EVOH blends were then hot-pressed at 230°C and 10 Mpa for 10 min and then cooled at room temperature.

Fourier transform infrared spectroscopy

Fourier transform infrared spectroscopic (FTIR) measurements of PA^{612}, EVOH, and PA^{612}/EVOH specimens were recorded on a Nicolet Avatar 320 FT-IR spectrophotometer at 25°C, wherein 32 scans with a spectral resolution 1 cm^{-1} were collected during each spectroscopic measurement. Infrared spectra of the film specimens were determined by using the conventional NaCl disk method. The 1,1,1,3,3,3-hexafluoro-2-propanol solutions containing the PA^{612}, EVOH and PA^{612}/EVOH were cast onto NaCl disk and dried at 60°C for 30 min, respectively. The cast films used in this study were prepared sufficiently thin enough to obey the Beer-Lambert law.

Wide angle X-ray diffraction

The wide angle X-ray diffraction (WAXD) measurements were conducted using a Siemens D5000D diffractometer equipped with a Ni-filtered CuK_α radiation operated at 35 kV and 25 mA. Each hot-pressed specimen with 1 mm thickness was maintained stationary at 25°C and scanned in the reflection mode from 2 to 40° at a scanning rate of 5° min^{-1}.

Isothermal crystallization process

Isothermal crystallization process was carried out using a TA Q100 differential scanning calorimetry.

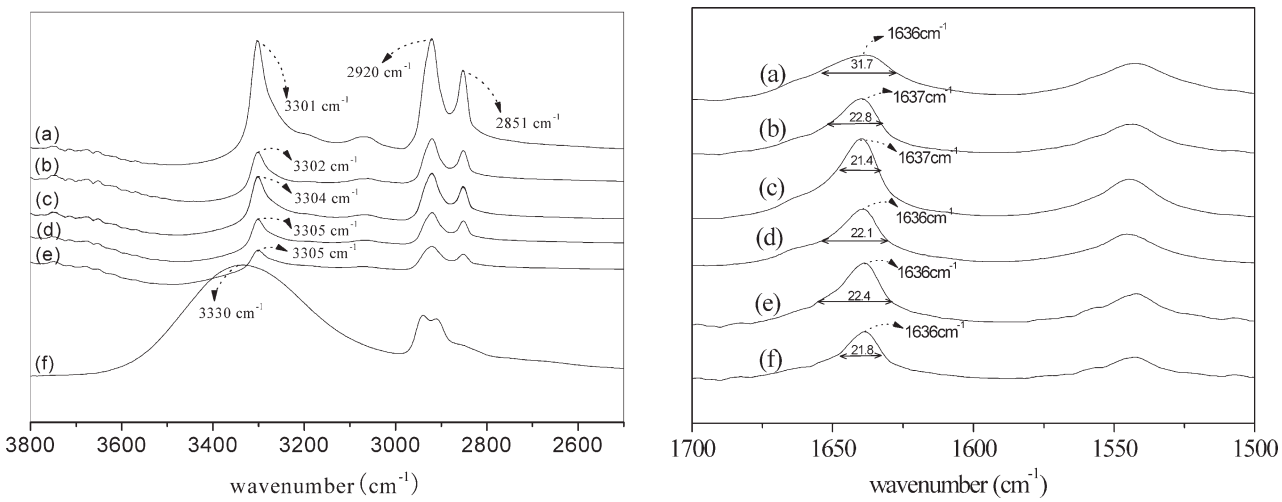

Figure 1 FTIR spectra of (a) PA^{612}, (b) $PA^{612}{}_7EVOH_1$, (c) $PA^{612}{}_5EVOH_1$, (d) $PA^{612}{}_3EVOH_1$, (e) $PA^{612}{}_1EVOH_1$ and (f) EVOH specimens determined at 25°C.

Calibration was carried out by using indium standard, with accuracy of temperature control being ± 0.1°C. All differential scanning calorimetry (DSC) experiments were performed under a nitrogen purge at a constant flow rate. Samples weighting 15 and 0.5 mg were placed in the standard aluminum sample pans for determinations of the crystallization process and melting temperature, respectively.

To assure that EVOH is in amorphous state (melt), in this study the crystallization temperatures are controlled higher than the T_m of EVOH and lower than that of PA^{612}. At these temperatures, PA^{612} crystallized selectively. The samples were rapidly heated at a rate of 50°C min^{-1} to 240°C above the melting temperature of blends, stayed there for 10 min to eliminate any residual crystals, then cooled to the designated crystallization temperature (T_c) at a rate of 80°C min^{-1} and remained isothermal until the crystallization was completed. The specimens were subsequently heated to 250°C at a rate of 10°C min^{-1}.

Dynamic mechanical analysis

The hot-pressed specimens with 0.2 mm thickness were sectioned into a rectangular strip with a dimension of 9 × 22 mm^2. All DMA experiments were operated at a frequency of 1 Hz, a heating rate of 3°C min^{-1} and in a temperature range from −50 to 150°C under N_2 atmosphere in the tensile mode.

Moisture absorption properties

Moisture absorption properties of PA^{612}, EVOH, and PA^{612}/EVOH specimens were carried out according to ASTM D570-98. The specimens were immersed in distilled water at 25°C. The samples were taken out of distilled water at regular intervals, gently wiped with tissue papers to remove the excess amounts of water. The wiped specimens were then weighed, repeatedly immersed in distilled water, wiped, and then weighed until their weights remained unchanged. The percentage increases in weight during the immersion in water were calculated as follows:

$$W_f\% = [(W_w - W_d)/W_d] \times 100$$

where W_f is the final increased weight percentage, W_w and W_d are the weights of the samples when they are dried and after moisture uptake, respectively. The values of moisture absorption were obtained based on the average results of five specimens.

RESULTS AND DISCUSSION

Fourier transform infrared spectra

Typical Fourier transform infrared spectra (FTIR) of PA^{612}/EVOH samples are summarized in Figure 1. Similar to those found in the literatures,[32,33] the distinguished absorption bands of PA^{612} specimens centered at 1540, 1636, 2851, 2920, and 3301 cm^{-1} are attributed to the motions of *N*-H bending vibration, hydrogen-bonded C=O stretching vibration, symmetric CH_2 stretching vibration, asymmetric CH_2 stretching vibration and hydrogen-bonded *N*-H stretching vibration present in PA^{612} molecules, respectively. An intense broad band centered at approximately 3330 cm^{-1} corresponding to hydroxyl stretching was found on the spectra of EVOH specimens, which is attributed to a distribution of intermolecular and/or intramolecular hydrogen-bonded OH dimmer and multimers.[34] After blending EVOH in PA^{612} resin, the peak wave numbers of the absorption bands corresponding to the hydrogen-bonded *N*-H stretching of PA^{612} molecules shift from 3301 to 3305 cm^{-1} as the EVOH contents of PA^{612}/EVOH

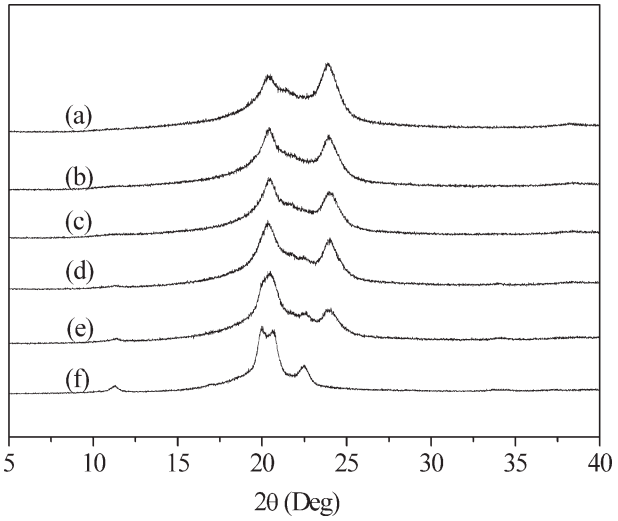

Figure 2 WAXS diffraction patterns of (a) PA^{612}, (b) $PA^{612}{}_7EVOH_1$, (c) $PA^{612}{}_5EVOH_1$, (d) $PA^{612}{}_3EVOH_1$, (e) $PA^{612}{}_1EVOH_1$, and (f) EVOH specimens.

specimens increase from 0 to 50 wt %. The absorption bands corresponding to the hydrogen-bonded *N*-H stretching shift to higher frequency but no free *N*-H stretching appears. This indicates that the original N-H groups bonded with C=O in PA^{612} could be destroyed and exists not as free but forms a new weaker hydrogen-bonded interaction with O—H groups in EVOH. In fact, the peak intensities of O—H stretching bands originally presented in EVOH specimen decrease with decreasing of EVOH contents.

Conversely, the half-height widths (Δw) shown on the C=O stretching bands of PA^{612}/EVOH specimens reduce significantly from 31.7 to 21.4 cm^{-1} as their EVOH contents increase from 0 to 16.7 wt %. At EVOH content higher than 16.7 wt %, their Δw values increase reversely with further increase in the EVOH contents of PA^{612}/EVOH specimens.

It is generally recognized that this reduction in Δw of the C=O stretching band can be attributed to the decreasing amounts of allowed C=O stretching vibrations.[35] Presumably, the decreasing allowed C=O stretching vibrations can be attributed to the gradually strengthened interaction between the carbonyl and hydroxyl groups in each PA^{612}/EVOH series specimens as their EVOH contents increase, respectively. Based on these premises, it is reasonable to suggest that the presence of EVOH in PA^{612} can interfere, break the hydrogen-bonded carbonyl groups originally presented in PA^{612} resins, and even form new interactions between the carbonyl/amide and hydroxyl groups as the weight ratios of PA^{612} to EVOH of PA^{612}/EVOH specimens increase. The strengthened interaction between the carbonyl and hydroxyl groups appears to reach the maximum level as the EVOH contents present in PA^{612}/EVOH specimens reach about 16.7 wt %.

Wide angle X-ray diffraction

Typical wide angle X-ray diffraction (WAXD) patterns and peak diffraction angles of PA^{612}/EVOH specimens are shown in Figure 2. Similar to the results found in Huang's investigation,[36] the main crystals of PA^{612} specimen melt-crystallized at 25°C are α form crystals, which correspond to two peak diffraction peaks centered at 20.4° and 24.1°. On the other hand, EVOH specimen exhibits an α form EVOH crystals diffraction pattern with four peak diffraction angles at 10.8°, 19.8°, 20.2°, and 22.5°, respectively. The characteristic diffraction patterns of α form EVOH[37] crystals become less demarcated after blending EVOH in PA^{612} resin. It is worth noting that the diffraction patterns of EVOH crystals can be barely found in PA^{612}/EVOH specimens, as the weight ratios of PA^{612} to EVOH are more than 5 (e.g., PA_7EVOH_1 and PA_5EVOH_1 samples).

These interesting FTIR and X-ray diffraction properties suggest that there is hydrogen bond interaction between PA^{612} and EVOH molecules, and this interaction force affect their crystallization properties each other. The fact that EVOH crystals almost disappear as their weight ratios of PA^{612} to EVOH are more than 5 is attributed that the hydrogen bond interaction between PA^{612} and EVOH molecules inhibit the crystal ability of EVOH.

Isothermal crystallization behavior of PA^{612} in PA^{612}/EVOH blends

The typical isothermal crystallization DSC curves of PA^{612} and PA^{612}/EVOH blends at five different crystallization temperatures are shown as Fig. 3. The shape of DSC curves for both pure PA^{612} and PA^{612}/EVOH blends is similar, and there is only one

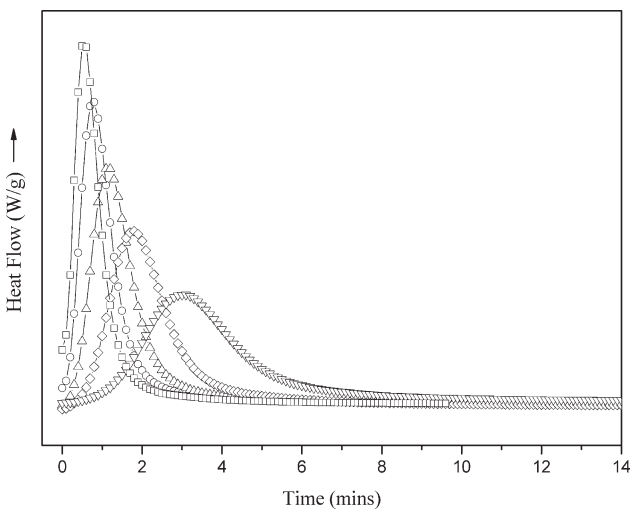

Figure 3 Isothermal crystallization DSC thermograms of $PA^{612}{}_7EVOH_1$ at 190°C (□), 192°C (○), 194°C (△), 196°C (◇), 198°C (▽).

TABLE II
Values of Isothermal Crystallization Parameters for PA^{612} in PA^{612}/EVOH Series Samples

Sample	T (°C)	$t_{1/2}$ (min)	t_p (min)	k	n
PA^{612}	190	0.17	0.15	1.23	3.96
	192	0.37	0.55	0.346	3.97
	194	0.70	0.77	0.102	3.94
	196	1.37	1.15	0.0237	3.89
	198	2.12	1.78	0.00370	3.88
$PA^{612}{}_7EVOH_1$	190	0.31	0.20	1.04	2.95
	192	0.52	0.39	1.04	2.86
	194	1.13	1.01	0.401	2.70
	196	2.09	2.02	0.440	2.69
	198	3.15	3.32	0.0290	2.78
$PA^{612}{}_5EVOH_1$	190	0.36	0.24	0.621	2.69
	192	0.58	0.43	0.161	2.67
	194	1.45	1.10	0.0298	2.55
	196	2.13	1.98	0.00530	2.57
	198	3.24	3.17	0.00300	2.57
$PA^{612}{}_3EVOH_1$	190	0.45	0.32	0.0210	2.11
	192	0.69	0.52	0.0103	2.02
	194	1.18	0.92	0.00260	2.00
	196	2.26	1.92	0.000300	1.96
	198	3.27	3.03	0.000200	1.98
$PA^{612}{}_1EVOH_1$	190	0.54	0.40	0.338	1.91
	192	1.00	0.73	0.0710	1.87
	194	1.67	1.55	0.0252	1.77
	196	2.88	2.65	0.0124	1.96
	198	3.43	3.22	0.000700	1.72

obvious crystallization enthalpy peak in each curve. However, the crystallization peaks of pure PA^{612} and PA^{612}/EVOH blends all become flatter and wider as their crystallization temperature increases. The peak crystallization time (t_p) taken at the maximum crystallization rate markedly increases with the crystallization temperature, although the interval of crystallization temperature is only 2°C. Presumably, as the crystallization is an exothermic process, the higher the crystallization temperature the more significant effect of temperature on t_p can be observed. As shown in Table II, from 190 to 198°C, the t_p of pure PA^{612} significantly increases from 0.15 to 1.78 min. However, after adding EVOH in PA^{612} resin, the PA^{612} needs more time to reach the maximum crystallization rate than the pure PA^{612} since the intermolecular interaction between PA^{612} and EVOH restricts the PA^{612} molecular chains' thermal motion to form crystals, and consequently delay the overall crystallization process.

The relative degree of crystallinity, X_t, as a function of crystallization time can be calculated using the following equation.[38]

$$X_t = \frac{\int_{t_0}^{t} \left(\frac{dH}{dt}\right) dt}{\int_{t_0}^{t_\infty} \left(\frac{dH}{dt}\right) dt} \quad (1)$$

where t_0 and t_∞ are the starting and finishing time of the crystallization, respectively, and H is the enthalpy of the crystallization process. Figure 4 presents the typical X_t as a function of crystallization time for PA^{612} in PA^{612}/EVOH specimens at various crystallization temperatures, wherein the $t_{1/2}$ defined as the time to reach $X_t = 50\%$ (see Table II). It is worth noting that $t_{1/2}$ of PA^{612} in pure PA^{612} and PA^{612}/EVOH series specimens increase as the crystallization temperature increases, respectively, wherein the $t_{1/2}$ of PA^{612} increase with the EVOH contents in PA^{612}/EVOH series specimens increasing. For instance, the $t_{1/2}$ of PA^{612} increases from 0.70 to 1.67 min as the EVOH content increase from 0 to 50 wt % at 194°C.

The curves are straight at the X_t range of 25–75%. This suggests the crystallization rate should be constant in this range. If C_r is the crystallization rate corresponding to the straight section of the curve, then the crystallization activation energy (E) can be evaluated using the Arrhenius equation[39]:

$$C_r = A \exp\left(\frac{-E}{RT}\right) \quad (2)$$

or

$$\ln C_r = \ln A - \frac{E}{RT} \quad (3)$$

where A is a temperature independence pre-exponential factor, R is the universal gas constant, and T is the absolute crystallization temperature. Plotting $\ln C_r$ versus $1/T$, a line can be obtained, so that the E can be obtained from its slope. The evaluated crystallization activation energies obtained from Figure 5 were summarized in Table III. As shown in Table III, E for PA^{612} increases with increasing the EVOH contents in PA^{612}/EVOH series specimens. For

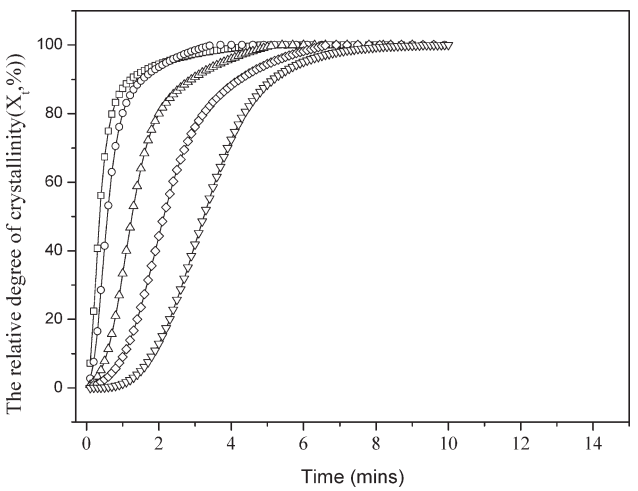

Figure 4 Plots of X_t versus crystallization time for $PA^{612}{}_7EVOH_1$ at 190°C (□), 192°C (○), 194°C (△), 196°C (◇), 198°C(▽).

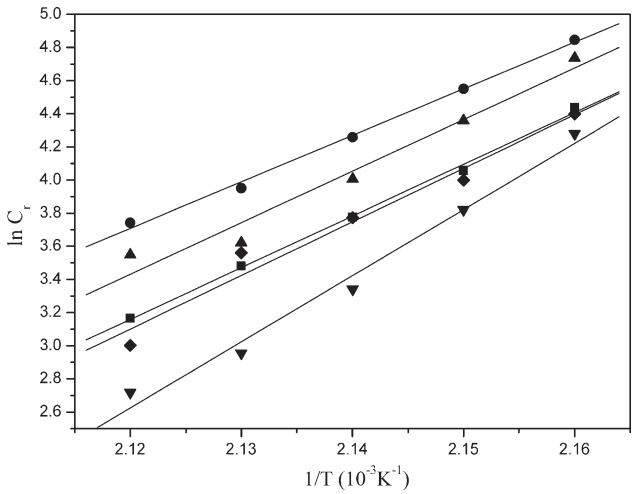

Figure 5 Plots of lnCr versus $1/T$ for PA^{612} (●), $PA^{612}{}_7EVOH_1$ (▲), $PA^{612}{}_5EVOH_1$ (■), $PA^{612}{}_3EVOH_1$ (◆), and $PA^{612}{}_1EVOH_1$ (▼).

instance, the E for PA^{612} increases from 233.3 to 293.7 KJ/mol as the EVOH contents increase from 0 to 50 wt %. Presumably, more activation energy is needed for PA^{612} crystallization in PA^{612}/EVOH blends since the introduction of EVOH resin in PA^{612} can retard the crystallization of PA^{612}.

The isothermal crystallization is analyzed on the basis of Avrami equation[40]:

$$1 - X_t = \exp(-kt^n) \tag{4}$$

or

$$\ln[-\ln(1 - X_t)] = \ln k + n \ln t \tag{5}$$

where X_t is the relative crystallinity, n is the Avrami exponent, depends on the type of nucleation and growth of the crystals; k is the overall kinetic rate constant and t is the crystallization time. The intercept and slop of ln[-ln(1-X_t)] versus ln$t$ yield k and n(see Fig. 6), respectively. The evaluated k and n are summarized in Table II. The rate constant (k) markedly decreases with the crystallization temperature increasing. The obtained Avrami exponent (n) ranges from 1.72 to 3.97, indicating that there was an average contribution of simultaneous occurrence of various types of nucleation and growth of crystallization. The crystallization mode of PA^{612} might be the mixture with two-dimensional, three-dimensional and diffusion-controlled growth with thermal nucleation. The higher the temperature, the slower the homogeneous nucleation and crystal growth rates become. So the values of n, depended on the type of nucleation and growth of the crystals, decrease with increasing crystallization temperature. The exponent n value of neat PA^{612} is quite close to 4, indicating that the crystallization process is governed by three-dimensional growth and homogeneous nucleation. Incorporation of EVOH leads to a decrease in exponent n from 3.96 to 1.91 at 190°C as the EVOH content increase from 0 to 50 wt %. The decrease of exponent n is probably attributed to the dimensionality of PA^{612} crystallization morphology decreases, and/or the type of nucleation changed from homogeneous to heterogeneous nucleation. Meanwhile, the Avrami exponent (n) of pure PA^{612} is almost the same with the crystallization temperature increasing. It is suggested that high temperature supplied more energy for folding of macromolecule chains to crystallize and destroying the existing crystal nuclei. Apparently, nucleation rate is predominant at higher temperature, and as a result, crystallization was completed in a lower crystallization rate at higher isothermal crystallization temperature. In fact, under employed temperature range, both nucleation mechanism and geometry of crystal growth of PA^{612} in PA^{612}/EVOH specimens are hardly affected by crystallization temperature. However, the presence of EVOH in PA^{612} resin significantly retards the crystallization growth of PA^{612}.

According to Hoffman-Weeks theory,[41] the equilibrium melting point may be deduced by plotting the observed apparent melting temperature T_m against the crystallization temperature T_c. The melting temperatures (T_m) of PA6 were measured after crystallization at various T_c. The equilibrium melting point is obtained by extrapolation of the resulting straight line to intersect the line $T_m = T_c$. The Hoffman-Weeks equation is as follow[42]:

$$T_m = \eta T_c + (1 - \eta) T_m^0 \tag{6}$$

Figure 7 shows the Hoffman-Weeks plots for PA^{612} in the bulk as well as in its blends with EVOH. It is seen that, in the blends, the equilibrium melting point of PA^{612} phase decreases steadily with EVOH content increasing. Thermodynamics predict that the chemical potential of the crystallizable polymer is decrease due to the presence of the miscible polymer, resulting in a decrease in the melting point.

TABLE III
Values of Crystallization Activation Energy (E) for PA^{612} in PA^{612}/EVOH Samples

Sample	PA^{612}	$PA^{612}{}_7EVOH_1$	$PA^{612}{}_5EVOH_1$	$PA^{612}{}_3EVOH_1$	$PA^{612}{}_1EVOH_1$
E(kJ/mol)	233.3	251.7	258.4	264.6	293.7

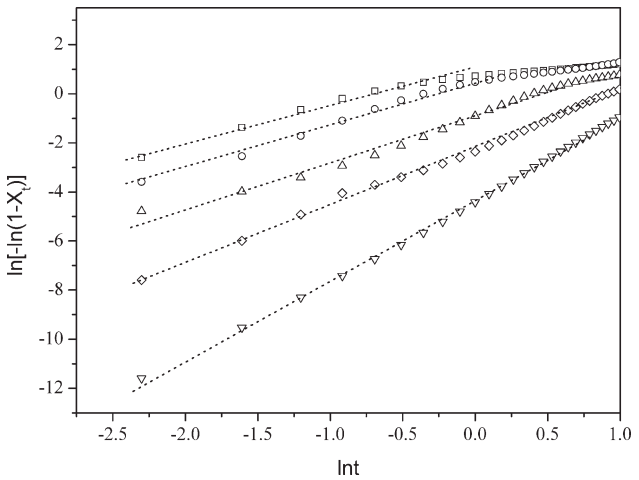

Figure 6 Plots of ln[-ln(1-X_t)] versus 1nt for $PA^{612}{}_7E$-VOH_1 at 190°C (□), 192°C (○), 194°C (△), 196°C (◇), 198°C(▽).

Characterization of PA^{612}/EVOH blends in the amorphous region

Figure 8 exhibits the temperature dependence of the tan δ curves of PA^{612}, PA^{612}/EVOH, and EVOH specimens. The tan δ transition is referred to the glass transition, which is associated with the relaxation of the main backbone chain and is determined by the tan δ peak. As suggested in the literatures,[41,43] the transition peaks near 50.2 and 72.3°C are recognized as the glass transition temperature (T_g) of PA^{612} and EVOH resins. The T_gs with peak temperature at 50.2°C and 72.3°C are found on the DMA thermograms for the PA^{612} and EVOH resins, respectively. It is worth noting that each blend sample exhibits only one tanδ peak due to the relaxation of amorphous fraction in the temperature range from 50.2°C to 72.3°C. Moreover, the T_g values increase with increasing EVOH content in PA^{612}/EVOH blends. The single tan δ transitions observed for the PA^{612}/EVOH specimens prepared in this study suggest that PA^{612} molecules are miscible with those EVOH molecules present in the amorphous phases at a limit degree,[44] since the tan δ transitions for PA^{612} and EVOH are very close. A dural T_g appears as EVOH content reaches 50 wt %. This indicates that PA^{612} and EVOH molecules are immiscible in amorphous phase as EVOH content is 50 wt %. As evidenced by WAXD analysis, EVOH crystals almost disappear as their weight ratios of PA^{612} to EVOH are more than 5, since the hydrogen bond interaction between PA^{612} and EVOH molecules inhibit the crystal ability of EVOH. So, PA^{612} molecules are part-miscible with those EVOH molecules present in the amorphous phases. However, as the EVOH content is more than 25 wt %, the strong crystallinity of PA^{612} and EVOH lead to negative effect on the miscibility between PA^{612} and EVOH in amorphous phase. In consequence, PA^{612} and EVOH molecules are immiscible in amorphous phase in $PA^{612}{}_5EVOH_5$ specimen.

Moisture absorption

Typical water absorption values of PA^{612}/EVOH samples are summarized in Figure 9. The PA^{612} specimen exhibit significantly lower water absorption (0.4 versus 21.7 wt %) than EVOH specimen. After blending EVOH in PA^{612}, the water absorption values of PA^{612}/EVOH specimens remain relatively unchanged initially with increasing the EVOH contents. For instance, the water absorption values of PA^{612}/EVOH specimens increase only slightly from 0.4 to 0.6 wt % as their EVOH contents

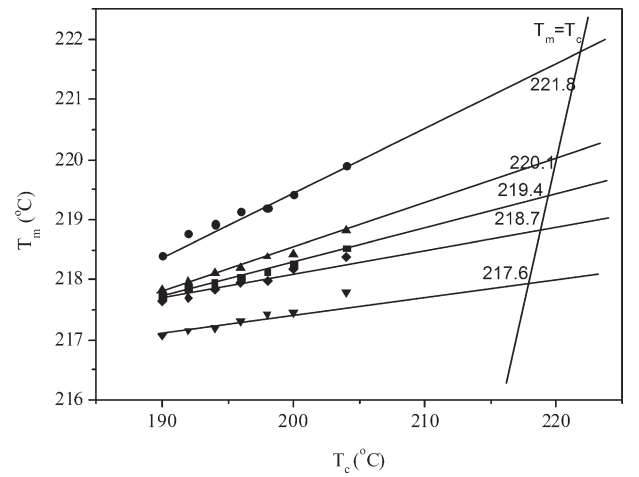

Figure 7 Equilibrium melting point (T_m^0) of PA^{612} in PA^{612} (●), $PA^{612}{}_7EVOH_1$ (▲), $PA^{612}{}_5EVOH_1$ (■), $PA^{612}{}_3EVOH_1$ (◆), and $PA^{612}{}_1EVOH_1$ (▼).

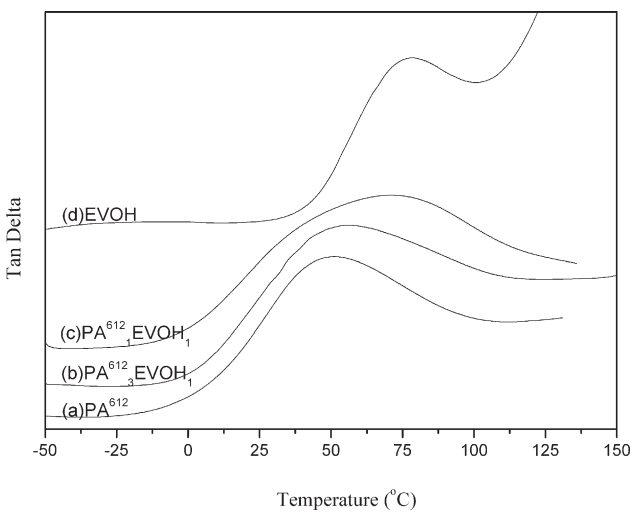

Figure 8 Temperature dependency of tan δ at 1 Hz for PA^{612}, PA^{612}/EVOH, and EVOH specimens.

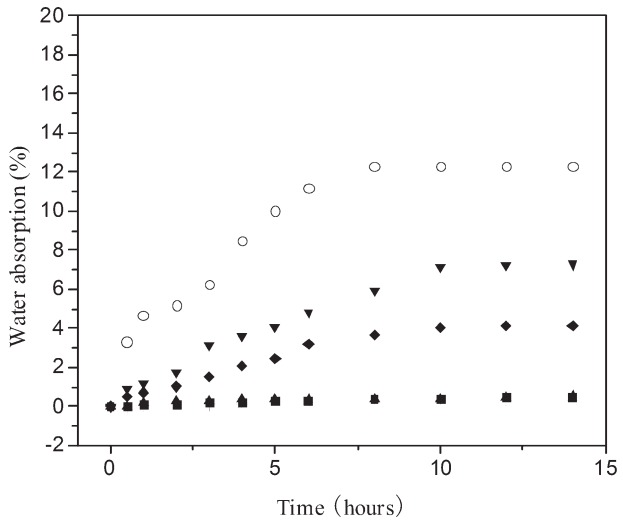

Figure 9 The values of water absorption of (a) PA^{612}(+), (b) $PA^{612}{}_7EVOH_1$(▲), (c) $PA^{612}{}_5EVOH_1$(■), (d) $PA^{612}{}_3EVOH_1$(◆), (e) $PA^{612}{}_1EVOH_1$(▼), and (f) EVOH(○) specimens at 25°C.

increase from 0 to 16.7 wt %. However, their water absorption values increase significantly from 0.6 to 22.3 wt % as the EVOH contents of PA^{612}/EVOH specimens increase from 16.7 to 100 wt %. EVOH is a hydrophilic synthetic polymer. The water absorption property of EVOH is significantly higher than that of PA^{612} [.[43] So, with the addition of EVOH, there is an increase in water absorption due to increase in hydroxyl groups.[45] As evidenced by FTIR and X-ray diffraction analysis, there is hydrogen bond interaction between PA^{612} and EVOH molecules, and EVOH crystals almost disappear as their weight ratios of PA^{612} to EVOH are more than 5. In addition, PA^{612} and EVOH molecules are miscible as the EVOH contents are equal to or less than 16.7 wt %. Therefore, the blends only exhibit the characteristic water absorption of PA^{612} as their EVOH contents are equal to or less than 16.7 wt %. As the EVOH contents are more than 16.7 wt %, EVOH was phase-separated from PA^{612} matrices due to crystallization. So the strong water absorption property of EVOH exhibits.

CONCLUSIONS

Hydrogen bonds interaction in the blends of PA^{612}/EVOH and the effect of the hydrogen bonds on characterization of PA^{612}/EVOH were systematically investigated. Fourier transform infrared spectra (FTIR) analysis showed the presence of EVOH in PA^{612} can interfere, break the hydrogen-bonded carbonyl groups originally present in PA^{612} resins, and even form new interactions between the carbonyl/NH and hydroxyl groups as the weight ratios of PA^{612} to EVOH of PA^{612}/EVOH specimens increase. The strengthened interaction between the carbonyl and hydroxyl groups appears to reach the maximum level as the EVOH contents present in PA^{612}/EVOH specimens reach about 16.7 wt %. One hand, this interaction between PA^{612} and EVOH some extent effects on their crystal phase. WAXD analysis showed that the crystallization properties of EVOH are inhibited significantly and even can be barely found in PA^{612}/EVOH specimens, as the weight ratios of PA^{612} to EVOH are more than 5. During the isothermal crystallization, the peak and half crystallization time of PA^{612} in PA^{612}/EVOH blends significantly increase with increasing crystallization temperature and EVOH content, while the degree of crystallinity and kinetic rate constant of PA^{612} in PA^{612}/EVOH blends markedly decrease with the crystallization temperature and EVOH content increasing. However, the crystallization activation energy for PA^{612} increases with increasing the EVOH contents in PA^{612}/EVOH series specimens. On the other hand, the hydrogen bonding between PA^{612} and EVOH also induce PA^{612} molecules are miscible with EVOH molecules to some extents in the amorphous phase. Furthermore, the characteristic moisture absorption of PA^{612}/EVOH specimen hardly appears as their EVOH contents are less than 16.7 wt %.

References

1. Olabisi, O.; Robeson, L. M.; Shaw, M. T. Polymer-Polymer Miscibility; Academic Press: New York, 1979.
2. Paul, D. R.; Newman, S. Polymer Blends; Academic Press: New York, 1978.
3. Lee, C. F. Polymer 2000, 41, 1337.
4. Kohan, M. I. Nylon Plastics; Wiley-Interscience: New York, 1973.
5. Uno, M.; Norton, L. J.; Kramer, E. J.; Oda, H. J Mater Sci 1998, 33, 853.
6. Ahn, T. O.; Kim, C. K.; Kim, B. K.; Jeong, H. M.; Hun, J. D. Polym Eng Sci 1990, 30, 341.
7. Koulouri, E. G.; Kallitsis, J. K. Polymer 1998, 39, 2373.
8. Incarnato, L.; Acierno, D.; Russo, P.; Malinconico, M.; Laurienzo, P. J Polym Sci Part B: Polym Phys 1999, 37, 2445.
9. Kuo, S. W.; Chang, F. C. Macromolecules 2001, 34, 5224.
10. Coleman, M. M.; Graf, J. F.; Painter, P. C. Specific Interactions and the Miscibility of Polymer Blends; Technomic Publishing: Lancaster, PA, 1991.
11. Coleman, M. M.; Lee, K. H.; Skrovanek, D. J. Macromolecules 1986, 19, 2149.
12. Kuo, S. W.; Huang, C. F.; Chang, F. C. J Appl Polym Sci 2006, 100, 1146.
13. Deimede, V. A.; Fragou, K. V.; Koulouri, E. G.; Kallitsis, J. K. Polymer 2000, 41, 9095.
14. Moolman, F. S.; Meunier, M.; Labuschagne, P. W.; Truter, P. A. Polymer 2005, 46, 6192.
15. Pearce, E. M.; Kwei, T. K.; Min, B. Y. J. Macromol Sci Chem A 1984, 21, 1181.
16. Ting, S. P.; Bulkin, B. J.; Kwei, T. K. J Polym Sci Polym Chem Ed 1981, 19, 1451.
17. Kuo, S. W.; Lin, H. C.; Chang, F. C. J Polym Sci Part B: Polym Phys 2006, 44, 673.

18. Huang, C. F.; Kuo, S. W.; Chang, F. C. Macromolecules 2006, 39, 300.
19. Wang, C. F.; Su, Y. C.; Chang, F. C. Angew Chem Int Ed 2006, 45, 2248.
20. Habi, A.; Djadoun, S. Eur Polym Mater 1999, 35, 483.
21. Habi, A.; Djadoun, S. Thermochimica Acta 2008, 469, 1.
22. Coleman, M. M.; Yang, X.; Painter, P. C. J Macromol Sci Part B 1993, 32, 295.
23. Ha, C. S.; Ko, H. G. Polymer 1997, 38, 1243.
24. Cui, L.; Yeh, J. T.; Wang, K.; Fu, Q. J. Polym Sci Part B: Polym Phys 2008, 46, 1360.
25. Zhang, L. L.; Goh, S. H.; Lee, S. Y. J Appl Polym Sci 1999, 74, 383.
26. Iriondo, P.; Iruin, J. J.; Fernandez-Berridi, M. J. Polymer 1995, 36, 3235.
27. Li, J.; He, Y.; Inoue, Y. J Polym Sci Part B: Polym Phys 2001, 39, 2108.
28. He, Y.; Asakawa, N.; Inoue, Y. J Polym Sci Part B: Polym Phys 2000, 38, 1848.
29. Chen, N. P.; Hong, L. Polymer 2002, 43, 1429.
30. Karos, W. J. Barrier Polymers and Structures; ACS Symposium Series 423, American Chemical Society, Washington, D.C. 1989.
31. Zhang, H. P.; Valentine, C.; Quigley, S. U. S.; Patent 2006; 0009582.
32. Yeh, J. T.; Yao, W. H.; Chen, C. C. J Polym Res 2005, 12, 279.
33. Coleman, M. M.; Yang, X.; Zhang, H.; Painter, P. C. J Macromol Sci Phys B 1993, 32, 295.
34. Person, W. B.; Zerbi, G. Vibrational Intensities in Infrared and Ramam Spectroscopy; Elsevier: New York, 1982.
35. Lagaron, J. M.; Gimenez, E.; Saura, J. J.; Gavara, R. Polymer 2001, 42, 7381.
36. Huang, J. H.; Li, Z. Y.; Qian, H. Mod Plasti Process Appl 2006, 18, 19.
37. Peng, S. W.; An, Y. X.; Chen, C.; Fei, B.; Zhuang, Y. G. Eur Polym Mater 2003, 39, 1475.
38. Cebe, P.; Hong, S. D. Polymer 1986, 27, 1183.
39. Hoffman, J. D.; Weeks, J. J. J Res Natl Bur Stand A 1962, 66, 13.
40. Nishi, T.; Wang, T. T. Macromolecules 1975, 8, 909.
41. Huo, P. P.; Cebe, P. Macromolecules 1993, 26, 3127.
42. Van Krevelen, D. W. Properties of Polymers; Elsevier: New York, 1976.
43. Mark, J. E. Polymer Data Handbook; Oxford University Press: New York, 1999.
44. Fried, J. R.; Karasz, F. E.; MacKnight, W. J. Macromolecules 1978, 11, 150.
45. Ramaraj, B.; Poomalai, P. J Appl Polym Sci 2005, 98, 2339.